PCCP

RSC Publishing

PAPER

View Article Online
View Journal | View Issue

Tandem cathode for proton exchange membrane fuel cells

Cite this: *Phys. Chem. Chem. Phys.*, 2013, **15**, 9326

Samira Siahrostami,[a] Mårten E. Björketun,[a] Peter Strasser,[b] Jeff Greeley[c] and Jan Rossmeisl*[a]

Received 8th April 2013,
Accepted 15th April 2013

DOI: 10.1039/c3cp51479j

www.rsc.org/pccp

The efficiency of proton exchange membrane fuel cells is limited mainly by the oxygen reduction reaction at the cathode. The large cathodic overpotential is caused by correlations between binding energies of reaction intermediates in the reduction of oxygen to water. This work introduces a novel tandem cathode design where the full oxygen reduction, involving four electron-transfer steps, is divided into formation (equilibrium potential 0.70 V) followed by reduction (equilibrium potential 1.76 V) of hydrogen peroxide. The two part reactions contain only two electron-transfer steps and one reaction intermediate each, and they occur on different catalyst surfaces. As a result they can be optimized independently and the fundamental problem associated with the four-electron catalysis is avoided. A combination of density functional theory calculations and published experimental data is used to identify potentially active and selective materials for both catalysts. Co-porphyrin is recommended for the first step, formation of hydrogen peroxide, and three different metal oxides – $SrTiO_3$(100), $CaTiO_3$(100) and WO_3(100) – are suggested for the subsequent reduction step.

Introduction

Pt is the best pure metal for catalyzing the oxygen reduction reaction (ORR) in proton exchange membrane fuel cells (PEMFCs). Nevertheless, there are several issues limiting the application of Pt-based PEMFCs. (1) Most importantly, the overpotential of the ORR is large.[1] (2) Consequently, the power obtained per unit mass of Pt is low. (3) The problem is further exacerbated by Pt scarcity. The global annual production of Pt corresponds to Pt for only four million fuel cell cars per year with present-day technology which is at least an order of magnitude too few.[2] This number could be increased if it was possible to obtain more power per gram of Pt used. Hence, in recent years great efforts have been devoted to enhancing the activity of Pt by reducing the energy losses and decreasing the Pt loading.

The four-electron reduction of O_2 ($O_2(g) + 4(H^+ + e^-) \rightarrow 2H_2O(l)$) involves at least three different adsorbed intermediates, O*, HO* and HOO*:

$$O_2(g) + (H^+ + e^-) + * \rightarrow HOO^* \quad (1)$$

$$HOO^* + (H^+ + e^-) \rightarrow H_2O(l) + O^* \quad (2)$$

$$O^* + (H^+ + e^-) \rightarrow HO^* \quad (3)$$

$$HO^* + (H^+ + e^-) \rightarrow H_2O(l) + *. \quad (4)$$

At high operating potentials, Pt sites are blocked by HO* due to their strong adsorption.[3] A simple "Sabatier analysis", in which the activity of the catalyst is plotted against the binding energy of HO*, shows that a 0.1 eV decrease in HO* binding, compared to Pt, would maximize the activity.[1]

Alloying with more abundant metals and forming Pt overlayers are the most promising strategies to electronically perturb the surface Pt atoms, so as to slightly weaken the binding of HO* and hence allow for a reduction of the Pt loading.[2,4–11] To date, the most active ORR catalysts have been reported by Stamenkovic *et al.* (Pt_3Ni)[6] and Greeley *et al.* (Pt_3Y),[11] whose works revealed an order of magnitude improvement over Pt(111). However, even on these surfaces, the ORR is far from the zero overpotential limit and the alloys tend to dissolve over time whereby the increased activity is lost. Unfortunately, Pt_3Y and Pt_3Ni appear to be located very close to the top of the Sabatier volcano, which suggests that state-of-the-art oxygen reduction catalysts are nearly as active as any electrocatalyst surface can ever become. In other words, there is probably little hope to find a catalyst surface that will be able to substantially reduce the overpotential. Moreover, there is no

[a] *Center for Atomic-scale Materials Design (CAMD), Department of Physics, Technical University of Denmark, DK-2800 Lyngby, Denmark. E-mail: Jan.Rossmeisl@fysik.dtu.dk*
[b] *Department of Chemistry, Chemical Engineering Division, Technical University Berlin, Strasse des 17. Juni 124, 16123 Berlin, Germany*
[c] *Center for Nanoscale Materials, Argonne National Laboratory, Argonne, IL 60439, USA*

obvious candidate to replace Pt in the highly corrosive environment surrounding the cathode.

It has been found that the high overpotential is caused by linear correlations between the binding energies of the reaction intermediates.[12–15] Because of these correlations it is impossible to simultaneously obtain perfect binding of all intermediates along a multi-electron reaction path. The catalytic performance ends up being a compromise between binding one intermediate not too weakly and another intermediate not too strongly. The problem is fundamental since there are universal scaling relationships, which are obeyed on any catalyst surface. As a result of the universal scaling, the energy difference between HO* and HOO* becomes essentially constant 3.2 ∓ 0.2 eV.[16] Since it takes two proton-coupled electron transfer steps to go from HOO* to HO* (reactions 2 and 3), a potential of at least 3.2 eV/2e = 1.6 V is needed to complete these reaction steps. However, the thermochemical limit is 1.23 V which means that even the best catalyst surfaces will have an overpotential of about $1.6 - 1.2$ V = 0.4 V.[16]

In this paper we suggest a radically new design of the fuel cell cathode that has the potential to overcome some of the major problems of the conventional oxygen electrode. It might eliminate the need for Pt, remove a large part of the overpotential, and exhibit improved stability. The conceptual idea will be thoroughly described in the next section. In brief, however, the idea is to divide the full four-electron transfer ORR (reactions (1)–(4)) into two two-electron transfer reactions, whose catalysis can then be optimized independently. In order to realize this, the cathode has to incorporate two distinct, highly selective, electrocatalysts. This introduces new catalysis-related challenges, which will be discussed in detail in the subsequent sections. A first attempt to identify catalysts that meet the new set of criteria will be made based on density functional theory (DFT) calculations. While rate limitations not directly related to the catalysis may remain, we believe that the proposed design represents an innovative idea well worth pursuing.

Tandem cathode – conceptual idea

As discussed in the introduction, the overpotential of the PEMFC cathode originates from the fact that the ORR is a four-electron transfer reaction with at least three intermediates (reactions 1–4) whose interactions with the catalyst have to be mutually optimized. For a two-electron transfer path such as the anode reaction (hydrogen oxidation) this problem does not arise since the reaction passes through only one intermediate (*e.g.* H*). The activity of the catalyst can be maximized if it binds the single intermediate with optimal strength, not too weakly and not too strongly as expressed by the classical Sabatier principle.[16] Hence if the ORR is divided into two two-electron reduction reactions, they and the overall reaction can in principle become as effective as the anode reaction. The possible set of two-electron transfer reactions is:[17]

$$O_2(g) + 2(H^+ + e^-) \rightarrow H_2O_2(l) \quad E_0 = 0.70 \text{ V} \qquad (5)$$

and

$$H_2O_2(l) + 2(H^+ + e^-) \rightarrow 2H_2O(l) \quad E_0 = 1.76 \text{ V}. \qquad (6)$$

Reaction (5) evolves hydrogen peroxide (H_2O_2) halfway through the ORR and includes only one intermediate, HOO*:

$$O_2(g) + * + (H^+ + e^-) \rightarrow HOO* \qquad (7)$$

$$HOO* + (H^+ + e^-) \rightarrow H_2O_2(l) + * \qquad (8)$$

and reaction (6) is the reduction of H_2O_2, also proceeding through one intermediate, HO*:

$$H_2O_2(l) + 2* \rightarrow 2HO* \qquad (9)$$

$$2HO* + (H^+ + e^-) \rightarrow H_2O(l) + HO* + * \qquad (10)$$

$$HO* + (H^+ + e^-) \rightarrow H_2O(l) + *. \qquad (11)$$

Reactions (5) and (6) have different standard potentials, 0.70 V and 1.76 V, respectively. This means that two distinct, spatially separated, cathodes are needed (henceforth referred to as cathode I and II). We call this construction a tandem cathode, a schematic of which is shown in Fig. 1. The two cathodes in Fig. 1 are not in direct electronic contact but only linked through the ion-conducting membrane, which means that a potential gradient can be formed between them. This system should thus be able to maintain two different (mixed) open circuit voltages (OCVs) as indicated in the cartoon. We would like to stress that the proposed design is qualitatively different from earlier dual site designs,[18,19] where the two types of active catalytic sites sit on a common highly conductive substrate.

A positive implication of the difference in standard potentials is the extended flexibility in the choice of stable catalyst materials. At cathode I the potential is lower than the usual 1.23 V, which means that materials with somewhat lower dissolution potential than Pt may be considered. Cathode II, on the other hand, works at a much higher potential where many oxides are stable. Similar to the anode reaction, the activities of catalyst candidates for cathode I and cathode II are maximized if they bind the

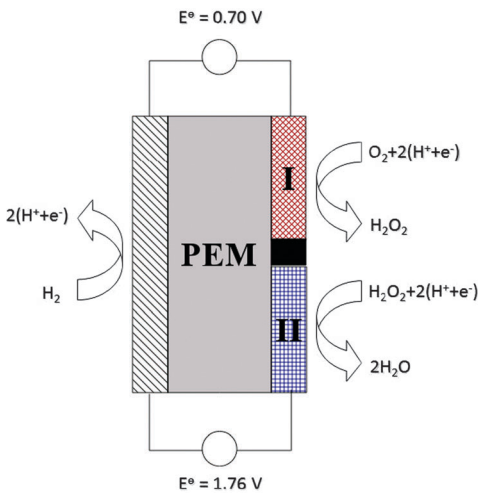

Fig. 1 Schematics of the PEMFC tandem cathode. The gray rectangle is the proton exchange membrane (PEM). The black hatched rectangle on the left represents the anode side while the red and blue crossed rectangles are cathodes I and II, respectively. The black small square eliminates electrical contact between cathodes I and II.

intermediates (HOO* and HO*) with optimal strength. This will be further explained and quantified in the next section.

The catalysis of the tandem cathode is distinctly different from that of the normal PEM cathode. If the tandem cathode would be realized it could potentially solve some of the major problems of traditional cathodes – the high overpotential and insufficient corrosion stability. In addition, the tandem cathode design has several other desirable features: (1) H_2O_2 can be electrochemically produced using a cheap catalyst.[20] (2) It can be synthesized in small amounts directly at the right place and right time and be used as fuel for the second cathode. (3) H_2O_2 is soluble and a powerful oxidizer over the whole pH range, with high oxidation potential (E_0 = 1.76 V).[21] (4) The electroreduction of liquid H_2O_2 at the second cathode takes place at a solid/liquid interface with a low activation barrier and fast kinetics.[22] However, the tandem cathode also gives rise to some challenges: H_2O_2 and its radicals represent a problem for the membrane, and the concentration of H_2O_2 needs to be relatively high to avoid transport limitations at cathode II. It is also worth mentioning that thermodynamically the potential one could get out of the two two-electron reactions is exactly the same as what one can get from the normal four-electron reaction. The net overpotential of the tandem cathode will be given by the sum of the individual overpotentials of the two-electron reactions.

Finally, in this theoretical paper, we will only consider the catalysis related issues introduced by the tandem cathode. Problems related to the engineering of the device will not be discussed.

Results and discussion

To be able to rationally design the catalysts in the tandem cathode, one first needs an understanding of the elementary reaction steps involved in the catalytic reactions. At cathode I, the oxygen reduction can follow either a two-electron path resulting in hydrogen peroxide formation, the desired product, or a four-electron path that ends with water.[23] A catalyst for cathode I should thus be efficient at producing H_2O_2 and at the same time be able to switch off both the decomposition reaction ($2H_2O_2(l) \rightarrow 2H_2O(l) + O_2(g)$) and the further reduction to water ($H_2O_2(l) + 2(H^+ + e^-) \rightarrow 2H_2O(l)$). For cathode II, on the other hand, a material that is able to reduce H_2O_2 to water and block the oxidation reaction would be a good candidate. In this section we use DFT simulations complemented with experimental data to identify catalysts that meet these necessary criteria – the analysis entails rather detailed mapping of reaction pathways. The two cathodes are treated separately; in the first subsection we try to optimize the catalysis of cathode I and then, in the second subsection, we address the catalysis of cathode II.

Cathode I

A wide variety of catalyst materials have already been introduced for H_2O_2 production in fuel cells.[24–32] H_2O_2 is selectively formed if and only if one can ensure that HOO* is the only intermediate (*cf.* reactions (7) and (8)). Among all the materials previously tested and introduced for H_2O_2 production, only three classes are found to favor HOO* compared to HO*. The three classes are: a gold surface with isolated Pd, Pt or Rh guest atoms;[33] graphitic materials doped with nitrogen;[34,35] and some metallo-porphyrins (M-porphyrins).[36–40] The common feature of all these materials is that their active sites are isolated, which prevents O–O bond breaking.

The Au–Pd alloy system has been extensively studied as an efficient catalyst for direct H_2O_2 synthesis.[41–46] Recently, Jirkovsky *et al.* predicted, by DFT calculations, that Au(111) alloyed with isolated Pd atoms should be selective and enhance the electrochemical production of H_2O_2.[33] To confirm the theoretical predictions and quantify the selectivity, they introduced $Au_{1-x}Pd_x$ nanoalloys with varying Pd content in a fuel cell cathode. These experiments demonstrated a pronounced increase in H_2O_2 formation for alloys with 8% Pd. Supported by their DFT modeling, they concluded that this low content corresponds to individual (guest) Pd atoms surrounded by Au host atoms.[33]

Some N-doped carbon based materials have also been shown to catalyze the two-electron pathway to H_2O_2.[34,35] Very recently, Fellinger *et al.* reported efficient, cheap and selective N-doped carbon for electrochemical production of H_2O_2.[20]

Heat-treated M-porphyrins supported on activated carbon are cheap alternatives for electrochemical production of H_2O_2 at room temperature.[47,48] In particular, several classes of Co-porphyrins have been introduced for electrochemical H_2O_2 production in the fuel cell.[49–54] A DFT study of ORR on Co-porphyrin (CoP) and Co-phthalocyanine (CoPc) reported by Sun *et al.* shows that O_2 only reduces to H_2O_2 without further reduction to H_2O on these catalyst surfaces.[55]

Among the three possible groups of catalysts, we have considered the M-porphyrins, which are graphitic materials functionalized with nitrogen and a transition metal (*cf.* Fig. 2). The active site of the M-porphyrin consists of the transition metal surrounded by four nitrogen atoms (*cf.* Fig. 2). Generally these materials are selective toward the full four-electron ORR,[56] but some of them do promote the desired two-electron pathway. In order to predict the activity of the catalyst and its selectivity towards either the two- or the four-electron process, we have calculated the binding energies of all potential adsorbates

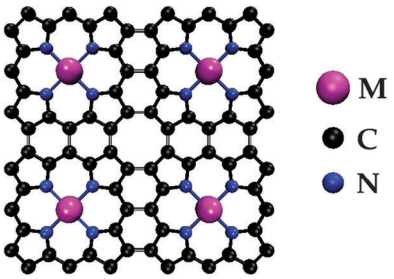

Fig. 2 Graphitic structure, functionalized with nitrogen and a transition metal atom. Neighboring nitrogen atoms are separated by three carbon atoms. The unit cell is repeated 2 × 2 times.

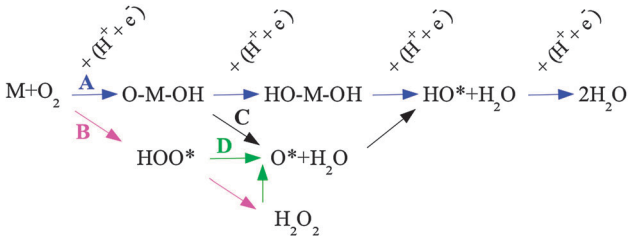

Scheme 1 Possible ORR pathways on M-porphyrin, used as cathode I.

along the ORR pathway (*cf.* Scheme 1) using DFT. Adsorption free energies have been obtained by adding entropy and zero-point energy corrections to the DFT energies.[57] Furthermore, we have accounted for water-induced stabilization of HO* and HOO*,[1] estimated to amount to ~0.3 eV per adsorbate.[56] In Fig. 3 we have plotted the free energies of the various ORR intermediates on the six investigated M-porphyrins (M = Cr, Mn, Fe, Co, Ni, and Cu) against the corresponding HO* free energies. Lower values reflect stronger coupling between M and the adsorbed species. The dashed lines indicate the free energy levels of O_2 and H_2O_2 at zero potential (4.92 eV and 3.52 eV, respectively, when considered relative to water). The window between these two levels (1.40 eV) is the free energy released when O_2 is reduced to H_2O_2 at zero potential. At a finite potential, the O_2 level will be shifted down $2eU$ relative to H_2O_2 (reaction (5)). If we divide 1.40 eV by $2e^-$, we arrive at 0.70 V, corresponding to the highest potential one could ever get from cathode I. On such an ideal catalyst the free energy diagram will be flat (the O_2, HOO* and H_2O_2 levels will be aligned) at the equilibrium potential. This means that the HOO* adsorption free energy will be half of the sum of the O_2 and H_2O_2 free energies *i.e.* 4.22 eV.

In Scheme 1 we have outlined several ORR pathways that might be accessible on the M-porphyrin. A is the unwanted four-electron pathway and B is the desired two-electron route. There are at least three criteria that have to be fulfilled in order for cathode I to effectively perform selective formation of H_2O_2. First, as mentioned earlier, the isolated active sites must mitigate O–O bond dissociation and favor HOO* compared to HO* + O* (O–M–OH). This is necessary in order to avoid the four-electron paths (A and C). Second, the active sites should promote reduction of HOO* to H_2O_2 (pathway B) during the second electron-proton transfer step. Therefore, it is crucial to find a catalyst with additional barriers for reduction of HOO* to O* + H_2O(l) and direct dissociation of H_2O_2 (pathways D). Third, the overpotential associated with formation of H_2O_2 has to be minimized, *i.e.* the free energy level of the HOO* intermediate has to be tuned.

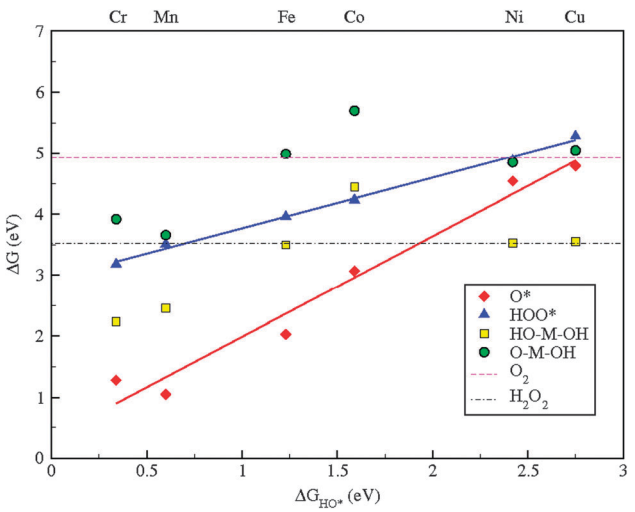

Fig. 3 Free energies at zero potential of different intermediates on six late transition metal (M) porphyrins, plotted against the free energy of HO*. The thermodynamic O_2 and H_2O_2 free energy levels are indicated as dashed and dashed-dotted horizontal lines, respectively.

The data in Fig. 3 suggest that the oxygen adsorption is strong on Cr-, Mn- and Fe-porphyrin, which is expected to promote O–O bond dissociation. This would result in formation of an O–M–OH intermediate after the first reduction step and then, after three subsequent proton electron transfer steps, lead to production of water. The latter part of the reaction could follow either pathway A, involving formation of HO–M–OH, or pathway C that goes through an O* + H_2O(l) intermediate (*cf.* Scheme 1).

Fig. 4 shows the free energy diagram (FED) for Fe-porphyrin. It clearly demonstrates that O–O bond dissociation runs in parallel with HOO* formation. Although HOO* formation occurs, the production of H_2O_2 will be strongly suppressed by the formation of O* + H_2O(l) which is more stable (pathway D). Even the small amount of H_2O_2 produced immediately converts into O* + H_2O(l) due to the strong thermodynamic driving force. The final product would thus always be water instead of H_2O_2. This prediction is in agreement with experimental findings[51,58,59] and earlier theoretical results[50,55] showing that the four-electron transfer process plays a dominant role in Fe-porphyrins. It is important to note that based on the FED in Fig. 4, the most probable pathway involves Fe + O_2(g), HOO*, O* + H_2O(l), HO* + H_2O(l) and 2H_2O(l), which is in agreement with the pathway proposed in the literature.[60,61]

In the case of Ni- and Cu-porphyrin, HOO* adsorption is weak and hence H_2O_2 is not formed at the favored potential.

Fig. 3 combined with the FED in Fig. 5 indicates that Co-porphyrin, as the only candidate, possesses the required features and hence could be both selective and active. The free energy of the O–Co–OH intermediate is 0.78 eV above the free energy of O_2, implying that pathway A is naturally avoided based on purely thermodynamic grounds. Consequently, Co-porphyrin becomes selective towards HOO* formation through pathway B. In the second electron–proton transfer step, HOO* is then reduced to H_2O_2. The calculated HOO* binding energy, including the stabilizing effect of the surrounding water, is 4.23 eV, which positions it almost exactly halfway between the O_2 and H_2O_2 levels and gives Co-porphyrin a theoretical over-potential of only 0.01 V.

Many experimental and theoretical studies suggest that the ORR follows a two-electron path, resulting in H_2O_2 as a final product, if Co-porphyrin containing *meso* substituents are used as catalysts.[38,50–55] Hence, we must assume the presence of an

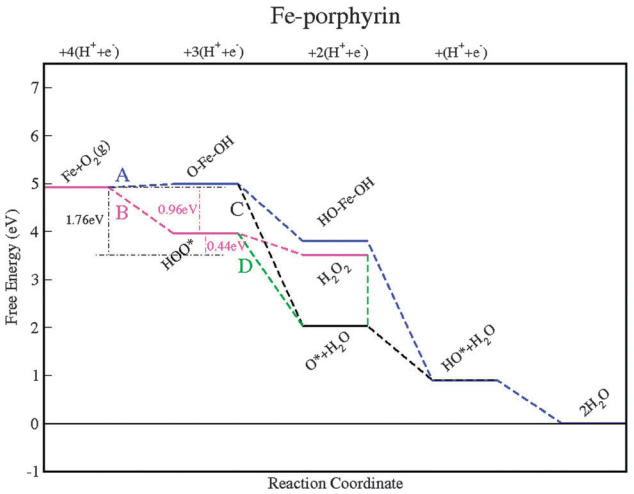

Fig. 4 Free energy diagram for O_2 reduction over Fe-porphyrin at zero potential, including different pathways. A and B are four- and two-electron transfer paths, respectively. Pathways C and D are four-electron transfer paths passing through O*.

additional barrier that prevents reduction of HOO* to O* + H_2O(l). As can be seen in Fig. 5, the free energy of O* + H_2O(l) is 0.45 eV lower than the free energy of H_2O_2. The barrier is thus not captured by pure thermodynamics, but is related to the kinetics. We believe that this kinetic barrier arises from the diversity of the chemical environment surrounding the oxygen atoms in HOO*. One of the oxygen atoms of HOO* binds to the metal in the porphyrin core while the other oxygen binds to hydrogen and to the first oxygen. Accordingly, two different kinetic barriers exist for transferring the second ($H^+ + e^-$) pair to these oxygen atoms. Addition of $H^+ + e^-$ to the first oxygen results in formation of H_2O_2 while addition to the second results in unwanted O* + H_2O(l). Based on the experimental results we conclude that the barrier

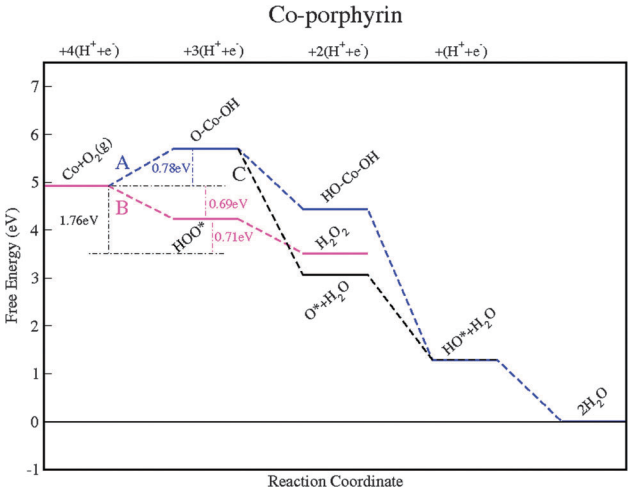

Fig. 5 Free energy diagram for O_2 reduction over Co-porphyrin at zero potential, including different pathways. A and C are four-electron transfer paths ending with water as a product. Pathway B is the desired two-electron transfer reaction. Pathway D in Scheme 1 has been omitted as it is considered irrelevant based on the experimental findings.

for transferring $H^+ + e^-$ to the first oxygen is lower. Co-porphyrin could therefore be both selective and active toward H_2O_2 production. The stability of Co-porphyrins is known to be an issue, as it is for almost any non-Pt catalyst.[40,62] However, several strategies such as heat treatment[62] and optimizing the membrane electrode assembly (MEA)[40] can be applied to increase the stability of the Co-porphyrin polymer structure and it could at least be used in a proof of concept device.

Cathode II

In the proposed design, H_2O_2 is used as an oxidant at cathode II. The use of H_2O_2 as an oxidant is in its early stages, however, recently, several types of fuel cells relying on this approach have been tested and reported.[52,63–66] Pd-based catalysts demonstrate both activity and selectivity toward H_2O_2 reduction.[22] For example, a thin adlayer of Pt over Pd was used by Kjeang *et al.* as the cathode of a membraneless microfluidic fuel cell to reduce H_2O_2.[63] Adams *et al.* compared $Pd_{0.25}Pt_{0.75}$/C with Pd/C, Pt/C and $Pd_{0.5}Pt_{0.5}$/C and found that it is more active toward H_2O_2 reduction.[67] Direct borohydride–hydrogen peroxide fuel cells (DBHPFCs) are based on BH_4^- oxidation at the anode and H_2O_2 reduction at the cathode in alkaline solution. Several catalysts have been tested and introduced for H_2O_2 reduction in the DBHPFC.[68–73] Among the suggested cathode catalysts, Pd,[68] MnO_2[72] and Pd–Ir electrodeposited on Ni foam[74] have exhibited high activities.

When trying to reduce H_2O_2, the main challenge is to prevent oxidation to O_2 (H_2O_2(l) → O_2(g) + 2($H^+ + e^-$)) while at the same time promoting reduction to H_2O (H_2O_2(l) + 2($H^+ + e^-$) → $2H_2O$(l)). The sum of the oxidation and reduction reactions results in decomposition of H_2O_2 and hence zero net current. In order to avoid the oxidation reaction, a number of constraints have to be imposed on the catalyst. In the following we will first study the reaction diagram for H_2O_2 (Scheme 2). This will give us a general idea of what has to be fulfilled. Then we will look at each constraint in detail and see what they mean in terms of binding of different reaction intermediates.

Scheme 2 displays the reaction paths including intermediates that might be involved on cathode II. Pathway A′ is the desired electrochemical reduction of H_2O_2 to H_2O. This reaction might be suppressed by the competing reaction paths B′, C′ and E′. In the first step, H_2O_2 might dissociate to O* and H_2O (path C′) or oxidize, to HOO* + H^+ + e^- (path B′). If the latter happens, there is still a chance that HOO* could be converted to 2HO* *via* channel D′ which

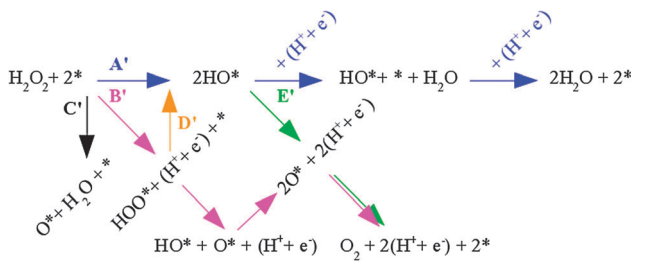

Scheme 2 Possible pathways on the surface of cathode II. Asterisks refer to active sites on the catalyst surface.

would bring the reaction back to A′. Pathway A′ could however be disrupted once again, this time by E′, which passes through 2O* before finally reaching O_2 + 2* after O* association.

In order for the reaction to proceed along the desired route, pathway A′, the side reactions, especially the irreversible ones, must be avoided. To steer the reaction in the right direction, the catalyst should first of all be efficient at cleaving the HO–OH bond in H_2O_2(l) so as to ensure formation of the 2HO* intermediate. Furthermore, it should suppress the O* formation and subsequent O* association (paths C′ and E′, and further down path B′). This requires weak binding of O*. Finally, we also want to minimize the overpotential associated with the reduction reaction. The overpotential is governed by the binding of OH to the catalyst surface so controlling the overpotential is a matter of tuning the free energy of HO*. The overpotential will be zero if the free energy diagram is totally flat at the equilibrium potential. The 2HO* and H_2O_2 levels will shift the same amount in response to a change in potential since the first step along A′ is a chemical reaction step and the two levels thus contain an equal number of electrons. The HO* level contains only half the number of electrons and the shift will therefore be half as big. As a result, an HO* adsorption free energy of 1.76 eV, when calculated at zero potential and relative to liquid water, will give zero overpotential.

Unfortunately, the catalysts mentioned in the beginning of this subsection all exhibit some oxidation and therefore at least partial decomposition of H_2O_2. In other words, the condition of weak O* binding is not satisfactorily met. If one would succeed in blocking the O* formation, the unfavorable reactions (H_2O_2(l) → H_2O(l) + O*, HO* → O* + H^+ + e^-, HOO* → HO* + O*, and 2O* → O_2(g) + 2*) would be switched off and the selectivity toward 2HO* and eventually formation of H_2O_2 would increase.

Recent calculations performed on a wide range of metal oxides including rutile, perovskite, spinel, rock salt, and bixbyite oxide surfaces[57,74] show that many metal oxides bind oxygen weakly. The high potential of cathode II, on the other hand, allows us to choose metal oxides since they are stable at high potentials. Another advantage of such oxides is that any effects of additional barriers to split the HO–OH bond would be negligible.[75] A key question is how weakly the O* must adsorb on the oxide surface in order to prevent the unwanted side reactions. It is also necessary to specify an optimal binding energy for HO*, which first of all makes sure the reaction passes through 2HO* and then minimizes the overpotential (maximizes the activity) of cathode II under that constraint. By comparing

$$H_2O_2 + 2(H^+ + e^-) \rightarrow 2HO^* + 2(H^+ + e^-) \rightarrow 2H_2O, \quad (12)$$

the desired reduction route and

$$H_2O_2 + 2(H^+ + e^-) \rightarrow 2O^* + 4(H^+ + e^-) \rightarrow O_2 + 4(H^+ + e^-), \quad (13)$$

the unwanted oxidation of H_2O_2, one can obtain more quantitative numbers for the two free energies. By shifting each level by $-neU$, where n is the number of electrons that each level needs to produce water and U is the electrode potential, one arrives at the following relation for the free energy levels of H_2O_2, HO* and O*:

$$2\Delta G_{O^*} - 4eU > \Delta G_{H_2O_2} - 2eU \geq 2\Delta G_{HO^*} - 2eU > 0 \quad (14)$$

or alternatively,

$$2\Delta G_{O^*} - 2eU > 3.52 \text{ eV} \geq 2\Delta G_{HO^*} > 0$$

which can be simplified to

$$\Delta G_{O^*} - eU > 1.76 \text{ eV} \geq \Delta G_{HO^*} > 0. \quad (15)$$

Relation (15) specifies the sought for optimal free energies of HO* and O*, and it shows that the metal oxide should simultaneously meet the following two conditions: first, the HO* free energy should be less than 1.76 eV and at the same time in order to minimize the overpotential and thereby maximize the activity it must be very close to 1.76 eV. Second, the O* free energy should exceed the H_2O_2 free energy level (3.52 eV) at the equilibrium potential. If this is fulfilled at the equilibrium potential it is automatically fulfilled at any lower potential. By applying these two conditions the unwanted reactions resulting in oxidation are avoided and the selectivity is increased.

Considering the condition of weak O* binding, one could pick oxides on the right hand side of the volcano plot (low coverage regime) presented in ref. 74. Fig. 6 shows the O* free energy of these oxides, along with that of WO_3 and two more stable perovskites ($BaTiO_3$, $CaTiO_3$),[76] as a function of the HO* free energy. Blue and black dashed lines indicate the free energies of H_2O_2 and HO* species, respectively. The free energy window between these two lines is the favorable free energy region for 2HO*. The solid red and black lines are the HO* and O* free energies. The distance between the black dashed line and the red volcano curve gives the overpotential for H_2O_2 reduction as a function of HO* free energy. At least three

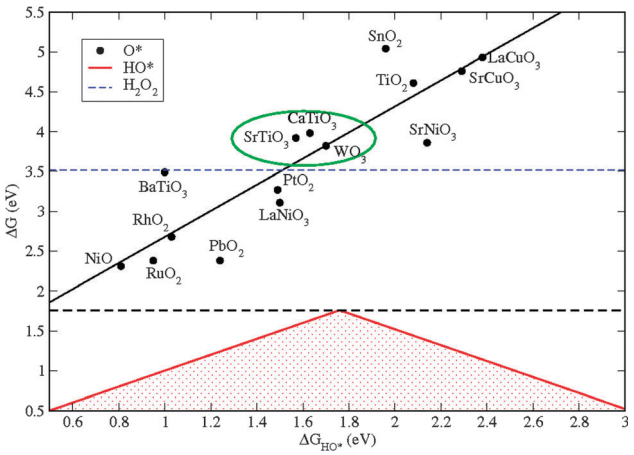

Fig. 6 O* and HO* free energies *vs.* HO* free energy for metal oxides in the low coverage regime; some data are adapted from ref. 74. The red dotted area specifies the volcano for HO*. The lowest allowed free energy of O* at the equilibrium potential is given by the blue dashed line and the highest allowed free energy of HO* is indicated by the black dashed line.

different categories of metal oxides can be identified in Fig. 6. They will be discussed below.

Metal oxides on the right side of the volcano have both high HO* and O* free energies ($\Delta G_{HO^*} > 1.76$ eV and $\Delta G_{O^*} > 3.52$ eV). This is inconsistent with the first condition but meets the second. For example, TiO_2 exhibits weak oxygen binding (4.61 eV) and thus fulfills the second condition. However, its HO* free energy (2.08 eV) is incompatible with the first. Metal oxides in this category are located far from the top of the volcano, implying huge overpotentials. If they would be used as catalysts, the H_2O_2 reduction would proceed extremely slowly.

Oxides on the left side, on the other hand, satisfy the first but not the second condition (RuO_2, for instance, binds oxygen only a little too weakly (2.38 eV) while it binds HO* strongly (0.95 eV)). As a consequence, the $H_2O_2 \rightarrow H_2O + O^*$ and $HO^* \rightarrow O^* + H^+ + e^-$ reactions might proceed in parallel with, and compete with, $H_2O_2 \rightarrow 2HO^*$. The simultaneous formation of O* and HO* species complicates the catalysis by making more than one intermediate available.

Five metal oxides in the middle are located at, or very close to, the top of the volcano. PtO_2 and $LaNiO_3$ have HO* free energies that place them close to the top of the volcano (1.49 eV and 1.50 eV, respectively), but their O* free energies are not satisfactory (ΔG_{O^*} = 3.27 eV for PtO_2 and ΔG_{O^*} = 3.11 eV for $LaNiO_3$). They thus suffer from basically the same limitations as the metal oxides in the second category. We are now left with three candidates, encircled by a green ellipsoid, that do fulfill both conditions; $SrTiO_3$ (ΔG_{HO^*} = 1.57 eV, ΔG_{O^*} = 3.92 eV), $CaTiO_3$ (ΔG_{HO^*} = 1.63 eV, ΔG_{O^*} = 3.98 eV) and $WO_3(100)$ (ΔG_{HO^*} = 1.70 eV, ΔG_{O^*} = 3.82 eV). The first two, $SrTiO_3$ and $CaTiO_3$, are cubic perovskites whereas WO_3 has a monoclinic structure. These oxides are expected to exhibit the smallest overpotentials for reaction (6), and the HO* free energies are at the same time located exactly in the window of permitted energies for this reaction. We thus suggest these three candidates for cathode II; they should be able to selectively reduce H_2O_2 to H_2O. Among these, $SrTiO_3$ and $CaTiO_3$ are attractive due to their satisfactory stability in severe environments.[77] Although they lack intrinsic electronic conductivity due to their wide band gaps, there are several strategies that could potentially give sufficient n-type conductivity:[78–80] immobilizing very thin films of the perovskites on conductive substrates, doping with suitable donor impurities that do not impede the ionic mobility, and making the perovskites non-stoichiometric or mixing them with conductive non-carbon materials like fluorine-doped SnO_2 are some possibilities.

Conclusions

In this paper we have introduced a new PEM fuel cell (PEMFC) design, the main purpose of which is to overcome fundamental problems associated with the oxygen reduction reaction (ORR) at the cathode, in particular the large overpotential. We have named it tandem cathode PEMFC since the usual monolithic cathode has been replaced by two cathodes working in series.

On a monolithic cathode, the ORR proceeds through four electron-transfer steps, passing three surface intermediates on its way from O_2 to H_2O. The binding energies of the surface intermediates obey universal scaling relationships and as a result they cannot be changed independent of each other. These correlations place a physical limitation on how small the overpotential can be made. In the new design, however, the ORR is separated into two distinct two-electron processes with only one intermediate each. Moreover, the two reactions occur on different, spatially separated, cathodes and they have different standard potentials. This removes the limitation caused by correlations among multiple intermediates.

On the first cathode, O_2 is supposed to reduce to H_2O_2 and the reaction should proceed through HOO*. On the second cathode we instead want to reduce H_2O_2 to H_2O and the reaction should proceed through HO*. The main challenges for the cathodes are to selectively form the desired intermediate and thus block unfavorable competing reactions, and to minimize the overpotential by tuning the binding energy of the intermediate. More specifically, HO* formation and further reduction to H_2O should be avoided on the first cathode (cathode I) and O* formation and oxidation to O_2 should be avoided on the second cathode (cathode II). Using water as a reference, the optimum free energies are 4.22 eV for HOO* on the first cathode and 1.76 eV for HO* on the second cathode.

Guided by the above specifications, we have used DFT calculations to identify selective catalysts with limited overpotentials for each cathode. We suggest Co-porphyrin for cathode I and three different metal oxides – $SrTiO_3(100)$, $CaTiO_3(100)$ and $WO_3(100)$ – for cathode II.

Finally, we would like to stress that the design proposed in this work should be rather generally applicable. A tandem approach could in principle be used to enhance the efficiency and selectivity of any reaction involving multiple electron-transfer steps. For instance, reduction of CO_2 to methane, methanol, or higher order hydrocarbons could probably benefit from a similar approach.

Computational details

The electronic structure calculations were performed using GPAW, a DFT code based on the projector-augmented wave (all electron, frozen core approximation) method.[81] The simulations were handled using the ASE package.[82] The RPBE exchange–correlation functional[83] was used in all calculations.

Three different types of systems – M-porphyrins, perovskite oxides and monoclinic $WO_3(100)$ – were modeled. The M-porphyrins were represented by periodic images of the sheets shown in Fig. 2, separated by 14 Å of vacuum in the *z*-direction. The spin-polarized calculations were performed and the Brillouin zone was sampled with a ($3 \times 3 \times 1$) Monkhorst–Pack *k*-point grid. The whole system was allowed to relax. The perovskites were confined to the cubic structure. Their surfaces were modeled by periodically repeated, 2×2 unit cells wide and 2 unit cells thick, slabs. The two top layers were allowed to relax. Periodic images were separated by 20 Å of vacuum in the direction perpendicular

to the surface. The Brillouin zone was sampled with a $(4 \times 4 \times 1)$ Monkhorst–Pack k-point grid. The $WO_3(100)$ surface was modeled by a 2×2 unit cell wide and 3 unit cells thick slab, and the two top layers were allowed to relax. This time periodic images were separated by 30 Å of vacuum in the direction perpendicular to the surface. The Brillouin zone was sampled with a $(3 \times 3 \times 1)$ Monkhorst–Pack k-point grid.

All geometric optimizations were carried out using the quasi-Newton minimization scheme and the calculations were considered converged when the residual forces were less than 0.05 eV $Å^{-1}$. In all calculations, the grid spacing was set to h = 0.18 Å as a tradeoff between computational efficiency and accuracy.

Acknowledgements

The authors acknowledge support from the Danish Center for Scientific Computing through grant HDW-1103-06, from the Catalysis for Sustainable Energy initiative funded by the Danish Ministry of Science, Technology and Innovation, and from the Danish Council for Strategic Research's Programme Commission on Strategic Growth-Technologies (NABIIT). Peter Strasser acknowledges support from the center of excellence in catalysis UNICAT funded by DFG and managed by the TU Berlin.

Notes and references

1 J. K. Nørskov, J. Rossmeisl, A. Logadottir, L. Lindqvist, J. R. Kitchin, T. Bligaard and H. Jonsson, *J. Phys. Chem. B*, 2004, **108**, 17886–17892.
2 I. E. L. Stephens, A. S. Bondarenko, U. Grønbjerg, J. Rossmeisl and I. Chorkendorff, *Energy Environ. Sci.*, 2012, **5**, 6744–6762.
3 A. S. Bondarenko, I. E. L. Stephens, H. A. Hansen, F. J. Perez-Alonso, V. Tripkovic, T. P. Johansson, J. Rossmeisl, J. K. Nørskov and I. Chorkendorff, *Langmuir*, 2011, **27**, 2058–2066.
4 H. Xin, A. Holewinski and S. Linic, *ACS Catal.*, 2012, **2**, 12–16.
5 M. Oezaslan and P. Strasser, *J. Power Sources*, 2011, **196**, 5240–5249.
6 V. R. Stamenkovic, B. Fowler, B. S. Mun, G. Wang, P. N. Ross, C. A. Lucas and N. M. Markovic, *Science*, 2007, **315**, 493–497.
7 W. Wakisaka, H. Suzuki, S. Mitsui, H. Uchida and M. Watanabe, *J. Phys. Chem. C*, 2008, **112**, 2750–2755.
8 W. P. Zhou, X. F. Yang, M. B. Vukmirovic, B. E. Koel, J. Jiao, G. W. Peng, M. Mavrikakis and R. R. Adzic, *J. Am. Chem. Soc.*, 2009, **131**, 12755–12762.
9 H. A. Gasteiger, S. S. Kocha, B. Sompalli and F. T. Wagner, *Appl. Catal., B*, 2005, **56**, 9–35.
10 I. E. L. Stephens, A. S. Bondarenko, F. J. Perez-Alonso, F. Calle-Vallejo, L. Bech, T. P. Johansson, A. K. Jepsen, R. Frydendal, B. P. Knudsen, J. Rossmeisl and I. Chorkendorff, *J. Am. Chem. Soc.*, 2011, **133**, 5485–5491.
11 J. Greeley, I. E. L. Stephens, A. S. Bondarenko, T. P. Johansson, H. A. Hansen, T. F. Jaramillo, J. Rossmeisl, I. Chorkendorff and J. K. Nørskov, *Nat. Chem.*, 2009, **1**, 552–556.
12 J. Rossmeisl, G. S. Karlberg, T. Jaramillo and J. K. Nørskov, *Faraday Discuss.*, 2008, **140**, 337–346.
13 J. Rossmeisl, A. Logadottir and J. K. Nørskov, *Chem. Phys.*, 2005, **319**, 178–184.
14 F. Abild-Pedersen, J. Greeley, F. Studt, J. Rossmeisl, T. R. Munter, P. G. Moses, E. Skulason, T. Bligaard and J. K. Nørskov, *Phys. Rev. Lett.*, 2007, **99**, 016105.
15 E. M. Fernandez, P. G. Moses, A. Toftelund, H. A. Hansen, J. I. Martinez, F. Abild-Pedersen, J. Kleis, B. Hinnemann, J. Rossmeisl, T. Bligaard and J. K. Nørskov, *Angew. Chem., Int. Ed.*, 2008, **47**, 4683–4686.
16 M. T. M. Koper, *J. Electroanal. Chem.*, 2011, **660**, 254–260.
17 F. Tian, R. Jinnouchi and A. B. Anderson, *J. Phys. Chem. C*, 2009, **113**, 17484–17492.
18 T. S. Olson, S. Pylypenko, P. Atanassov, K. Asazawa, K. Yamada and H. Tanaka, *J. Phys. Chem. C*, 2010, **114**, 5049–5059.
19 Y. Liang, Y. Li, H. Wang, J. Zhou, J. Wang, T. Regier and H. Dai, *Nat. Mater.*, 2011, **10**, 780–786.
20 T. P. Fellinger, F. Hasche, P. Strasser and M. Antonietti, *J. Am. Chem. Soc.*, 2012, **134**, 4072–4075.
21 J. M. Campos-Martin, G. Blanco-Brieva and J. L. G. Fierro, *Angew. Chem., Int. Ed.*, 2006, **45**, 6962–6984.
22 D. Cao, L. Sun, G. Wang, Y. Lv and M. Zhang, *J. Electroanal. Chem.*, 2008, **621**, 31–37.
23 P. Vassilev and M. T. M. Koper, *J. Phys. Chem. C*, 2007, **111**, 2607–2613.
24 I. Yamanaka, T. Onizawa, S. Takenaka and K. Otsuka, *Angew. Chem., Int. Ed.*, 2003, **115**, 3781–3783.
25 I. Yamanaka, *Catal. Surv. Asia*, 2008, **12**, 78–87.
26 I. Yamanaka, T. Hashimoto, R. Ichihashi and K. Otsuka, *Electrochim. Acta*, 2008, **53**, 4824–4832.
27 I. Yamanaka, S. Tazawa, T. Murayama, R. Ichihashi and N. Hanaizumi, *ChemSusChem*, 2008, **1**, 988–990.
28 L. Fu, S. You, F. Yang, M. Gao, X. Fang and G. Zhang, *J. Chem. Technol. Biotechnol.*, 2010, **85**, 715–719.
29 C. Samanta, *Appl. Catal., A*, 2008, **350**, 133–149.
30 E. Lobyntseva, T. Kallio, N. Alexeyeva, K. Tammeveski and K. Kontturi, *Electrochim. Acta*, 2007, **52**, 7262–7269.
31 K. Ke, T. Hatanaka and Y. Morimoto, *Electrochim. Acta*, 2011, **56**, 2098–2104.
32 C. M. Sanchez-Sanchez and A. J. Bard, *Anal. Chem.*, 2009, **81**, 8094–8100.
33 J. Jirkovsky, I. Panas, E. Ahlberg, M. Halasa, S. Romani and D. J. Schiffrin, *J. Am. Chem. Soc.*, 2011, **133**, 19432–19441.
34 R. A. Sidik and A. B. Anderson, *J. Phys. Chem. B*, 2006, **110**, 1787–1793.
35 K. A. Kuark and A. B. Anderson, *J. Phys. Chem. C*, 2009, **113**, 6730–6734.
36 P. Vasudevan, Santosh, N. Mann and S. Tyagi, *Transition Met. Chem.*, 1990, **15**, 81–90.
37 J. Zagal, M. Pgez, A. A. Tanaka, J. R. dos Santos and C. A. Linkous, *J. Electroanal. Chem.*, 1992, **339**, 13–30.
38 E. Song, C. Shi and F. C. Anson, *Langmuir*, 1998, **14**, 4315–4321.
39 F. Jaouen, E. Proietti, M. Lefevre, R. Chenitz, J. Dodelet, G. Wu, H. T. Chung, C. M. Johnston and P. Zelenay, *Energy Environ. Sci.*, 2011, **4**, 114–130.

40 J. M. Ziegelbauer, T. S. Olson, S. Pylypenko, F. Alamgir, C. Jaye, P. Atanassov and S. Mukerjee, *J. Phys. Chem. C*, 2008, **112**, 8839–8849.
41 J. K. Edwards, B. E. Solsona, P. Landon, A. F. Carley, A. Herzing, C. J. Kiely and G. J. Hutchings, *J. Catal.*, 2005, **236**, 69–79.
42 J. K. Edwards and G. J. Hutchings, *Angew. Chem., Int. Ed.*, 2008, **47**, 9192–9198.
43 J. K. Edwards, B. Solsona, E. N. Ntainjua, A. F. Carley, A. A. Herzing, C. J. Kiely and G. J. Hutchings, *Science*, 2009, **323**, 1037–1041.
44 H. C. Ham, G. S. Hwang, J. Han, S. W. Nam and T. H. Lim, *J. Phys. Chem. C*, 2009, **114**, 12943–12945.
45 H. C. Ham, G. S. Hwang, J. Han, S. W. Nam and T. H. Lim, *J. Phys. Chem. C*, 2010, **114**, 14922–14928.
46 J. Li, T. Ishihara and K. Yoshizawa, *J. Phys. Chem. C*, 2011, **115**, 25359–25367.
47 K. Otsuka and I. Yamanaka, *Electrochim. Acta*, 1990, **35**, 319–322.
48 I. Yamanaka, T. Onizawa, H. Suzuki, N. Hanaizumi and K. Otsuka, *Chem. Lett.*, 2006, 1330–1331.
49 R. R. Durand and F. C. Anson, *J. Electroanal. Chem.*, 1982, **134**, 273–289.
50 L. Mao, K. Arihara, T. Sotomura and T. Ohsaka, *Electrochim. Acta*, 2004, **49**, 2515–2521.
51 R. Chen, H. Li, D. Chu and G. Wang, *J. Phys. Chem. C*, 2009, **113**, 20689–20697.
52 Y. Yamada, Y. Fukunishi, S. Yamazaki and S. Fukuzumi, *Chem. Commun.*, 2010, **46**, 7334–7336.
53 B. Su, I. Hatay, A. Trojanek, Z. Samec, T. Khoury, C. P. Gros, J. M. Barbe, A. Daina, P.-A. Carrupt and H. H. Girault, *J. Am. Chem. Soc.*, 2010, **132**, 2655–2662.
54 C. J. Chang, Z. H. Loh, C. Shi, F. C. Anson and D. G. Nocera, *J. Am. Chem. Soc.*, 2004, **126**, 10013–10020.
55 S. Sun, N. Jiang and D. Xia, *J. Phys. Chem. C*, 2011, **115**, 9511–9517.
56 F. Calle-Vallejo, J. I. Martinez and J. Rossmeisl, *Phys. Chem. Chem. Phys.*, 2011, **13**, 15639–15643.
57 J. Rossmeisl, Z. W. Qu, H. Zhu, G. J. Kroes and J. K. Nørskov, *J. Electroanal. Chem.*, 2007, **607**, 83–89.
58 A. L. Bouwkamp-Wijnoltz, W. Visscher and J. A. R. Van Veen, *Electrochim. Acta*, 1998, **43**, 3141–3152.
59 D. Ricard, A. Didier, M. L'Herb and B. Boitrel, *C. R. Chim.*, 2002, **5**, 33–36.
60 A. B. Anderson and R. A. Sidik, *J. Phys. Chem. B*, 2004, **108**, 5031–5035.
61 J. Chlistunoff, *J. Phys. Chem. C*, 2011, **115**, 6496–6507.
62 V. S. Bagotzky, M. R. Tarasevich, K. A. Radyushkina, O. A. Levina and S. I. Andrusyova, *J. Power Sources*, 1977, **2**, 233–240.
63 E. Kjeang, A. G. Brolo, D. A. Harrington, N. Djilali and D. Sinton, *J. Electrochem. Soc.*, 2007, **154**(12), B1220–B1226.
64 S. Yamazaki, Z. Siroma, H. Senoh and T. Ioroi, *J. Power Sources*, 2008, **178**, 20–25.
65 Y. Shao, S. Zhang, C. Wang, Z. Nie, J. Liu, Y. Wang and Y. Lin, *J. Power Sources*, 2010, **195**, 4600–4605.
66 Y. Bing, H. Liu, L. Zhang, D. Ghosh and J. Zhang, *Chem. Soc. Rev.*, 2010, **39**, 2184–2202.
67 B. D. Adams, C. K. Ostrom and A. Chen, *J. Electrochem. Soc.*, 2011, **158**(4), B434–B439.
68 J. Ma, Y. Sahai and R. G. Buchheit, *J. Power Sources*, 2010, **195**, 4709–4713.
69 D. A. Finkelstein, J. D. Kirtland, N. Da Mota, A. D. Stroock and H. D. Abruna, *J. Phys. Chem. C*, 2011, **115**, 6073–6084.
70 C. Ponce de Leon, F. C. Walsh, C. J. Patrissi, M. G. Medeiros, R. R. Bessette, R. W. Reeve, J. B. Lakeman, A. Rose and D. Browning, *Electrochem. Commun.*, 2008, **10**, 1610–1613.
71 U. B. Demirci, *J. Power Sources*, 2007, **172**, 676–687.
72 W. Haijun, W. Cheng, L. Zhixiang and M. Zongqiang, *Int. J. Hydrogen Energy*, 2010, **35**, 2648–2651.
73 D. Cao, D. Chen, J. Lan and G. Wang, *J. Power Sources*, 2009, **190**, 346–350.
74 I. C. Man, H. Su, F. Calle-Vallejo, H. A. Hansen, J. I. Martinez, N. G. Inoglu, J. Kitchin, T. F. Jaramillo, J. K. Nørskov and J. Rossmeisl, *ChemCatChem*, 2011, **3**, 1159–1165.
75 A. Vojvodic, F. Calle-Vallejo, W. Guo, S. Wang, A. Toftelund, F. Studt, J. I. Martinez, J. Shen, I. C. Man, J. Rossmeisl, T. Bilgaard, J. K. Nørskov and F. Ablid-Pedersen, *J. Chem. Phys.*, 2011, **134**, 244509.
76 F. Calle-Vallejo, J. I. Martinez, J. M. Garcia-Lastra, M. Mogensen and J. Rossmeisl, *Angew. Chem., Int. Ed.*, 2010, **49**, 7699–7701.
77 F. Noll, W. Munch, I. Denk and J. Maier, *Solid State Ionics*, 1996, **86–88**, 711–717.
78 A. Murashkina, V. Maragou, D. Medvedev, V. Sergeeva, A. Demin and P. Tsiakaras, *J. Power Sources*, 2012, **210**, 339–344.
79 D. Neagu and J. T. S. Irvine, *Chem. Mater.*, 2011, **23**, 1607–1617.
80 W. Dong, Y. Guo, B. Guo, H. Liu, H. Li and H. Liu, *Mater. Lett.*, 2012, **88**, 140–142.
81 J. J. Mortensen, K. Kaasbjerg, S. L. Frederiksen, J. K. Nørskov, J. P. Sethna and K. W. Jacobsen, *Phys. Rev. Lett.*, 2005, **95**(21), 216401.
82 Atomic Simulation Environment (ASE), URL: https://wiki.fysik.dtu.dk/ase, Center for Atomic Scale Materiale Design (CAMD), Technical University of Denmark, Lyngby.
83 B. Hammer, L. B. Hansen and J. K. Nørskov, *Phys. Rev. B: Condens. Matter Mater. Phys.*, 1999, **59**(11), 7413–7421.

